

International Conference on Space Optics—ICSO 2018

Chania, Greece

9–12 October 2018

Edited by Zoran Sodnik, Nikos Karafolas, and Bruno Cugny



Uniformity and wavefront control of optical filters

Michael Vergöhl

Chris Britze

Stefan Bruns

Andreas Pflug

et al.



ics0 proceedings



Uniformity and wavefront control of optical filters

Michael Vergöhl^{a*}, Chris Britze^a, Stefan Bruns^a, Andreas Pflug, Jennifer Zimara^b, Bernd Schäfer^b, Klaus Mann^b, Volker Kirschner^c

^aFraunhofer Institute for Surface Engineering and Thin Films, (IST), Bienroder Weg 54E, 30108 Braunschweig, Germany; ^bLaser Laboratorium Göttingen, Germany, ^cEuropean Space Research and Technology Centre, The Netherlands

ABSTRACT

The present paper addresses uniformity effects in demanding dielectric optical coatings. The origins of spectral resonant wavefront errors (WFE) induced by non-uniformities in complex dielectric filters are investigated in detail. The coating is a broad-band beamsplitter with a high reflectance between 400 and 900 nm and a high transmittance between 920 and 2300nm. The WFE can significantly be reduced with an optimized design. A new setup based on Hartmann-Shack sensors measures the spectrally dependent WFE in the visual spectral range. The paper presents a method for referencing the measured data. The experimental WFE maps obtained by spectral Hartmann-Shack measurements agree well with the expected spectra taken from spectral photometric measurements and the coating design. The paper also addresses coatings on curved surfaces. A band pass filter centered at 670 nm on the convex side of a lens was developed. Using a combination of a sub-rotation and special uniformity masks, a very low spectral shift of the passband position overall the lens surface could be demonstrated. The deposition concept and mask design, respectively, are developed via simulation studies based on a simulation approach shown in [10]. Extension of the model framework by plasma simulation and a concept for computing deposition profiles on moving 3D substrates was required for solving the problem.

Keywords: Broadband beam splitter, magnetron sputtering, spectral wavefront error, curved substrate surface, lens coating, band pass filter

1. INTRODUCTION

It is well known that low wavefront errors (WFE) are important for diffraction limited optical systems, e.g. [1]. Spectral wavefront errors in dielectric coatings in the near infrared region (1.1-2.4 μm) for the use in the Magdalena Ridge Observatory Interferometer were investigated by Nyland [2]. Recently it was observed that in a dielectric beamsplitter coating, surprisingly large, resonant like errors of the reflected wavefront occur at specific wavelengths [3]. Lappschies presented a phase optimized design for the Euclid Beamsplitter [4]. The existence of such resonances of the reflected or transmitted wavefront at specific wavelengths is not new. Already Baumeister [5] stated in his book that “as measured on an interferometer at other than the design wavelength, the figure of an optical surface with multilayer coatings with non-uniform thicknesses may be fallacious”. These wavelength effects become especially important when the thin film designs get more complex and thicker. The origin is an imperfect lateral uniformity of the coating. In the present study, a broad-band beam splitter with a high reflectance from 400 to 900 nm and a high transmittance from 920 to 2300 nm was developed. Different designs have been analyzed with regard to spectral performance and also to the spectral wavefront error. For this purpose, a measurement setup has been installed to monitor the spectral dependence of the wavefront error on components with up to 120mm diameter.

A second objective presented in this paper is the deposition of a band pass filter centered at 670 nm onto the convex surface of a spherical lens. Application of interference filters directly onto curved optical components instead using separate coatings on flat substrates is advantageous since it reduces the number of internal reflections in the optical device. However, with PVD it is challenging to achieve homogeneous coatings on curved substrates. Naturally, the deposition rate on tilted substrates decreases with the cosine of the angle between surface normal and direction of deposition flux [11]. In case of the investigated lens shape this yields a 7% decrease in film thickness at the most off-centered positions. In contrast, maintaining the functional wavelength of the band pass filter for off-centered beam positions would require a controlled *increase* of the deposition rate.

A concept for realization of this controlled non-homogeneity was developed via prior simulation studies based on the reactor model of the EOSS® coater presented in [10]. This model is extended by PIC-MC plasma simulation, an algorithm for projection of the modelled deposition flux onto moving 3D substrates and by a fitting algorithm for optimization of the mask geometry. As a result, a combination of a sub-rotation with a shaping mask was used to deposit the lens by magnetron sputtering with the EOSS® turntable coater. The deposited layers show the required linear film thickness increase from center toward border position of the lens surface. A demonstrator coated with the band pass filter shows virtually no spectral shift of the passband position over the whole lens surface.

*Michael.vergoehl@ist.fraunhofer.de; phone +49 531 2155 500; fax +49 531 2155 900; www.ist.fraunhofer.de

2. SPECTRAL WAVEFRONT ERROR IN COATINGS

2.1 Setup for beam splitter and lens coating

The principal setup of the beam splitter arrangement shows Figure 1, left. The angle of incidence is 30° and the aperture of the chief ray is $F\# > 20$. The component shall have a reflectivity of $R > 98\%$ (average polarization) within 400-900 nm and a transmittance of $T > 92\%$ in the NIR range (920-2300 nm). Moreover, the resulting wavefront error (WFE) shall be less than 20 nm RMS. Note that, since a real wavefront can have various shapes, there is generally no simple relation the root-mean-square wavefront error (RMS-WFE) and the peak-to-valley wavefront error (PV-WFE). Usually the PV-WFE is a few times larger than the RMS-WFE. For the present work, it will be assumed that the RMS-WFE is 1/6 of that of the PV-WFE, following also the theoretical work in [6]. According to the setup, the reflected wavefront has to be determined only in the short wave spectral range (400-900nm). The intended diameter of the component is 120 mm, however for the coating the substrate diameter was chosen to 140 mm. The thickness of the substrate is 12 mm.

Also shown in Figure 1 (right) is the geometry for the lens analysis. The lens is a plano-convex lens with a curvature of 25,7mm. The bandpass was deposited on the convex side. In the present study, no backside coating was applied. For the bandpass filter, the angle of incidence is of high importance. The AOI is 0° in the center of the lens and 16° at a position 4,8mm from lens center, respectively. To measure the transmittance spectrum of the lens, an Ulbricht sphere assessment of a Perkin Elmer Lambda 900 spectrophotometer was used. Additional apertures realize a parallel light beam with low angular divergence. Tilting the lens by an angle of 8° realizes the required 16° angle of incidence to the lens surface.

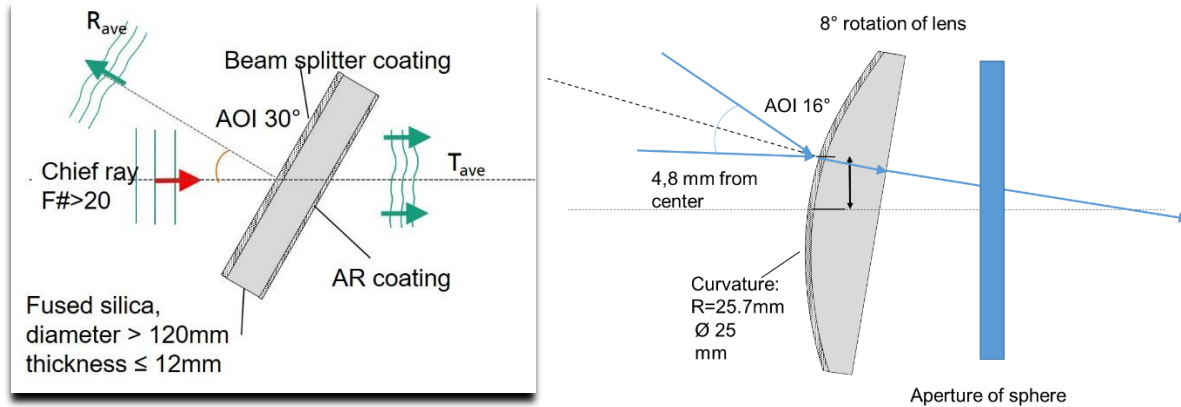


Figure 1: Left: Scheme of the beam splitter arrangement. **Right:** Shape of the lens and light beam geometry.

2.2 Design of coating including wavefront error

McLeod [7] has shown that wavefront errors in coatings can be calculated from the reflected or transmitted phase values. Therefore the reflected spectral phase has to be calculated for different thicknesses according to the assumed non-uniformity of the coating. If the thickness on one side of the coating is too small or too thick, the incoming wave hits the surface at different positions. This induces another phase shift. In order to define a constant phase when the wave hits the surface, another compensation air layer has to be implemented on top of the coating. The compensation layer must have the opposite thickness profile, i.e. if the coating is 100 nm thinner on one side, the air layer must be 100 nm thicker. The wavefront error spectra for the designs shown later were calculated by this method. In [12] it was shown that the group delay can be used to design coatings with specific targets regarding wavefront properties.

According to this finding, the group delay was used for the further design optimization runs. For the final calculation of the WFE, the phase difference method given by McLeod was used as mentioned before.

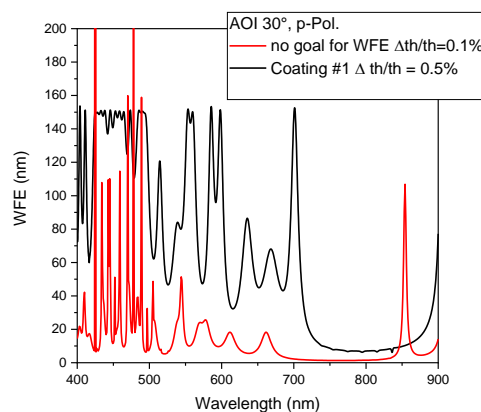


Figure 2: Simulation of WFE (p.v.) of a standard coating and of an optimized coating. Note the different non-uniformity values (0.1% for the standard design versus 0.5% for an optimized design Coating #1 used for the calculations).

A number of designs have been calculated according to the requirements of the optical performance and the targeted WFE. In general, it turned out that the higher the refractive index difference between low and high index materials, the smaller the WFE, assuming identical non-uniformities of the coating. However, since a high reflectance is required for wavelengths

below 450nm, Ta₂O₅ was used as the high index material. Figure 3 compares two results for the calculated WFE. “Filter 1_4” indicates a standard beam splitter coating, i.e. when using no target for the WFE. “Filter 7_12b” indicates a coating with optimized WFE. It is obvious that although for the non-optimized coating a non-uniformity of 0.1% is assumed, the WFE has even larger resonances. The WFE uniformity scales linearly with the non-uniformity, i.e. the non-optimized coating must have a 5 times better uniformity (here: 0.1% and 0.5%, respectively) to obtain similar wavefront errors.

3. EXPERIMENTAL SETUP

3.1 Deposition of coatings

For the deposition of the coating, the EOSS[®] coater developed by Fraunhofer IST [8, 9] was used (Figure 4). The coating is performed by magnetron sputtering in a rotating turntable setup. Up to 10 substrates of 200mm diameter can be placed on the turntable which rotates at 250 rpm. As sputtering sources, dual rotatable magnetrons are used. The oxidation takes place at the plasma source supplied with oxygen gas. We used Silicon targets for the low index material and a mixture of metallic and oxide compound for the high index material. In the present paper, Ta₂O₅ layers were deposited for the high index material as stated before. An optical broadband monitor controls the coating during the process. Beam splitter #1 was deposited with time control only; which is possible because of the extremely high stability of the coating process. Beam splitter #2 was deposited with indirect optical monitoring, using different monitor glasses.

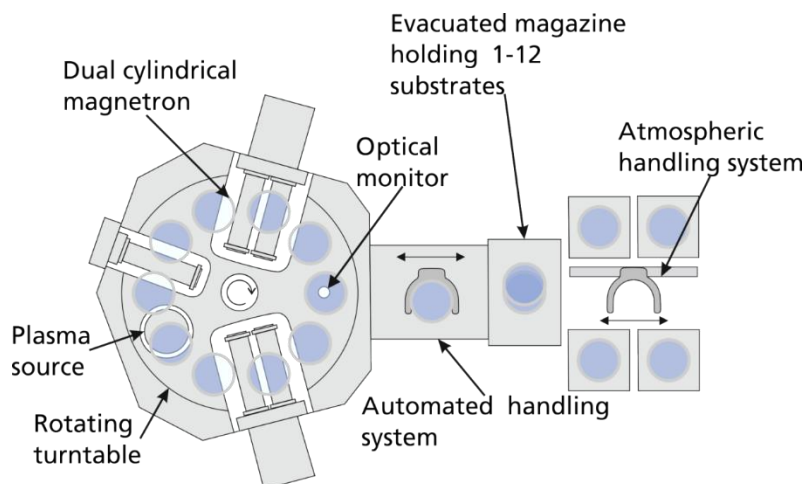


Figure 3: Coating system EOSS[®] used for the deposition of the coatings [7,8].

3.2 Measurement of wavefront error

For the spectrally resolved measurement of wavefront errors of optical components a setup based on a Hartmann-Shack wavefront sensor was established. As broad-band light source a laser driven plasma lamp (Energetiq, EQ99) is employed, followed by a fibre coupled grating monochromator ($f/2$, Technologie-Manufaktur GmbH, Germany), which can be tuned from 400nm to 800nm with a spectral bandwidth of 2nm. Different optics including aspheric lenses were used for expansion (5x) and collimation of the beam, accomplishing a collimated beam diameter of 140mm dia. at the sample position. Both the reflected and the transmitted wavefront can be monitored with a high-resolution large-area Hartmann-Shack wavefront sensor (FOV 36mmx24mm, $f=40$ mm, Laser-Laboratorium Göttingen). In the present work only the reflected wavefront was registered. For absolute calibration of the data a plane wavefront is provided by reflection from a flat substrate with an rms wavefront error of 2.5nm (dia. 150mm, Zygo), representing the lower limit for the absolute accuracy of the measurement system. The setup is depicted in Figures 4 and 5.

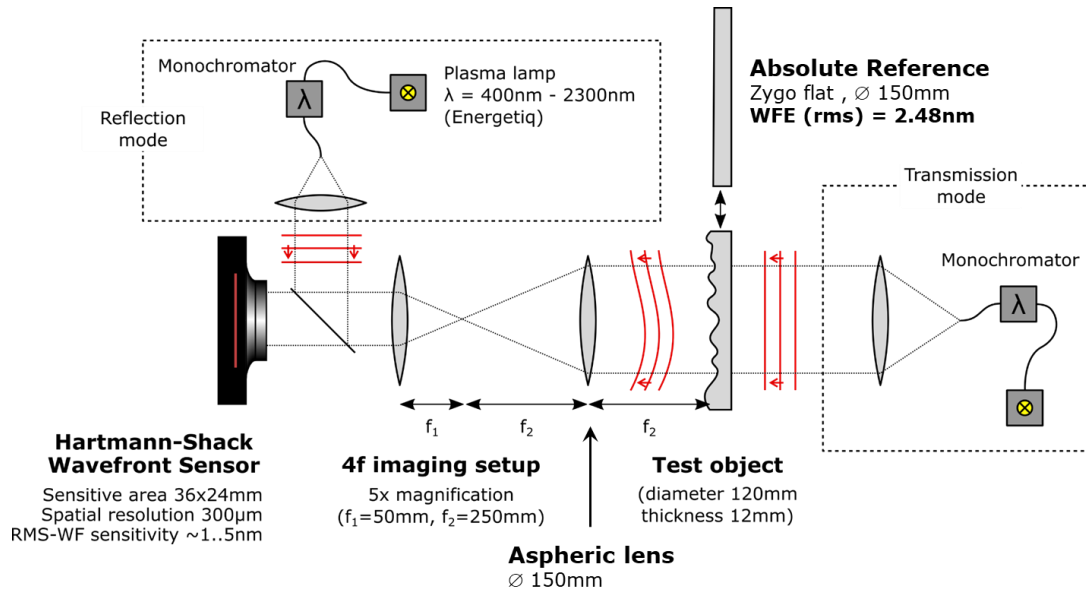


Figure 4: Experimental setup for reflection and transmission measurements.

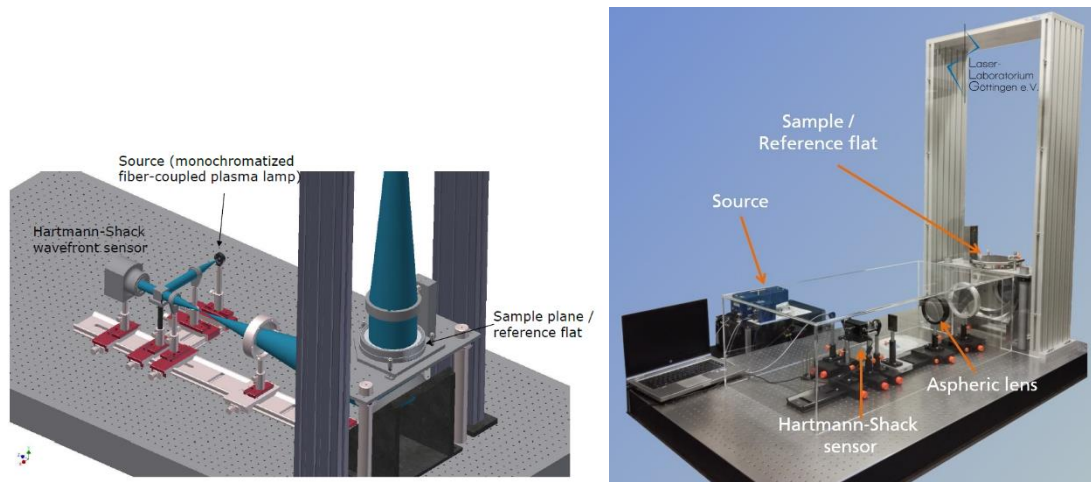


Figure 5: Setup for spectrally resolved wavefront measurements ($\lambda = 400$ nm - 800nm, $\Delta\lambda = 2$ nm, sample size up to 140mm dia.)

4. RESULTS AND DISCUSSION

4.1 Beam splitter coating

This paper presents two different beam splitter coatings. They were deposited on quartz substrates of 140 mm diameter. Beam splitter coating #1 consist of 110 layers of SiO_2 and Ta_2O_5 . The total thickness is 9500 nm. The calculated group delay within 400-900nm is less than 130 fsec at 0° and less than 140 fsec at 30° AOI. The beam splitter coating #2 consists of 150 layers with a total thickness of around 14,2 μ m. The group delay within 400-900nm is less than 150 fsec at 0° AOI. At 30° AOI, it is less than 150 fsec and less than 180 fsec for p and s-polarization, respectively. The coating #2 was thicker in order to fulfill the spectral requirements around the transition between the reflecting and the transmitting range. That needed more layers and resulted in a higher thickness. While the beam splitter #1 had an antireflective coating and another

stress compensation layer on the back side, the coating #2 was applied identically on both sides. That means the coating #2 also had an anti-reflecting function in the NIR range. The resulting reflectance spectrum of coating #2 shows Figure 6. In the short wavelength range, the reflectance is well above the specified value of 98%. Some reduction is observed around 750 nm is caused by the specific design, i.e. the penetration depth of the light at that wavelength is higher than at the shorter wavelengths. In the NIR range, the oscillations are not exactly reproduced in the measurement. Mainly the difference is due to the limited spectral resolution of the measurement. Around the band edge at 900 nm, the angular divergence of the spectrometer leads to a broadening of the spectra. The precise determination of transmittance or reflectance required another measurement setup. Therefore, a self-built spectrometer was used to measure the transmission of the filter. That system has a spectral bandwidth of 0.2nm and an angular divergence of 0.25°. The resulting spectra are shown in Figure 7 for the s- and the p-polarized beam, respectively. A very good agreement between theory and measurement is obvious. The very tight specification ($T_{s,p} < 1\%$ @ $\lambda < 900$ nm, $T_{s,p} > 80\%$ @ $\lambda > 900$ nm, where s,p are the s- and the p-polarized components, respectively) is fulfilled.

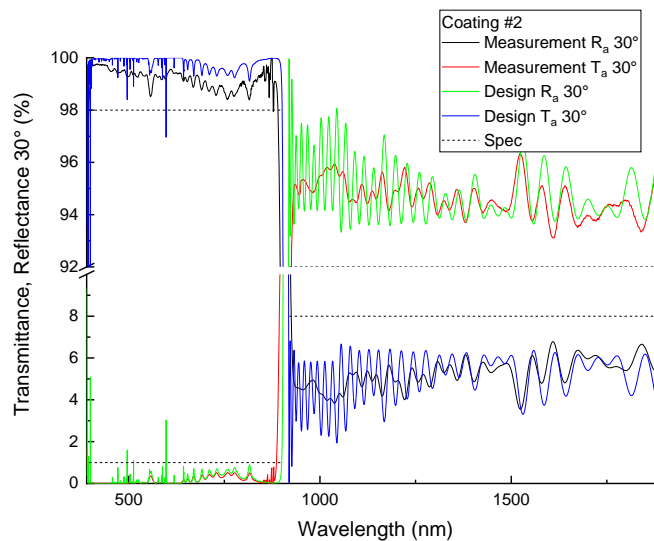


Figure 6: Reflectance and transmittance (unpolarized) of the beam splitter coating #2.

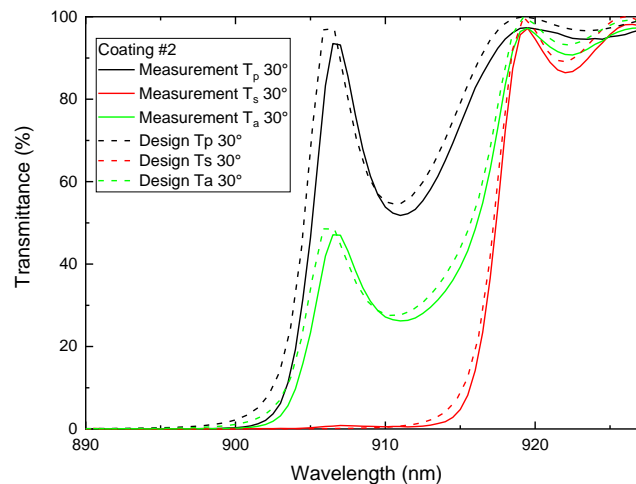


Figure 7: Detail transmittance spectrum of beam splitter coating #2 around the band edge at 900nm. The spectrum was measured by an own built spectrometer with a low angular divergence of 0.25°.

To determine the lateral uniformity of the coating, the transmittance of the sample was measured with a spectrometer (Perkin Elmer Lambda 950) at different positions over the sample. These data were obtained at normal incidence in order to avoid the spectral broadening. The measurement was performed normal and also along the arc of motion of the substrate. The non-uniformity on 120mm was better than $\pm 0,125\%$. Also from ellipsometric measurement on single layers (thickness 300nm), these non-uniformities are confirmed. The standard deviation of the thickness measurement was less than 0.05%.

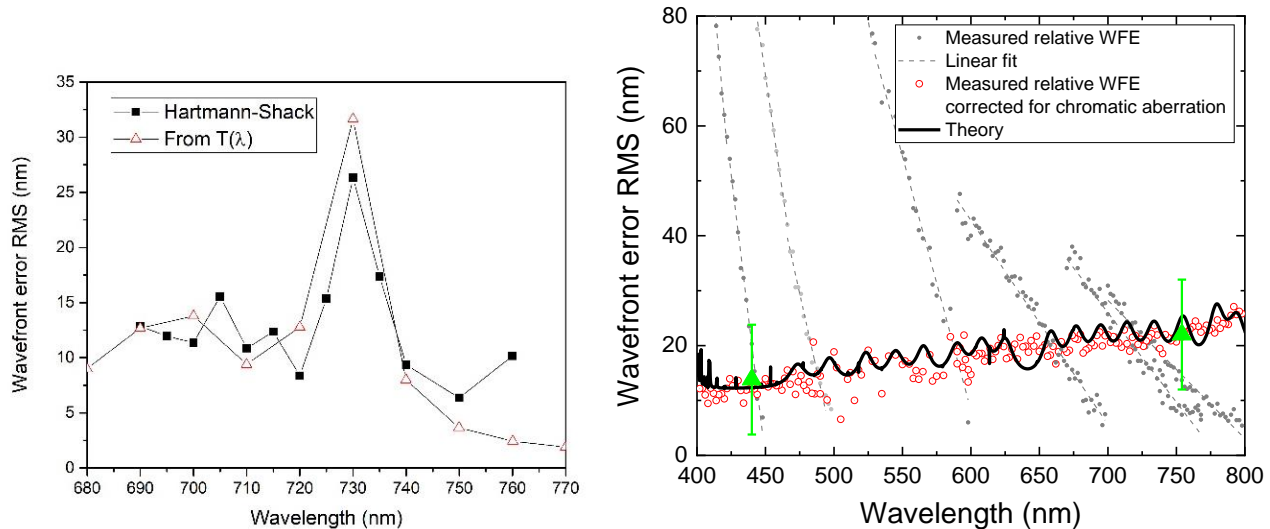


Figure 8: Left: Result of spectral WFE from Hartmann-Shack measurements of beam splitter coating #1 with a higher non-uniformity of 0.5%. Red triangles: Calculated from theory. Black boxes: Spectral WFE with self-reference method. **Right:** Wavefront errors determined by the self-reference method (Red circles: After chromatic error compensation in comparison with the theory (black line) and absolute wavefront errors at 440 and 754 nm (green triangles).

In Figure 8 (left), the relative WFE of the coating #1 is presented. Note that the data in the left diagram only shows the relative and not the absolute WFE, i.e. substrate bending and effects of the surface reference plane are neglected in that diagram. The figure 8 right, on the other hand, presents absolute data, including bending of the substrate, substrate surface roughness and the non-uniform “air layer”.

The theoretical WFE was calculated by the following way: Assuming that the low and the high index material show identical thickness distribution, the non-uniformity of the coating was determined from a special feature of the coating. In the case of the coating #1 it was the wavelength position of the band edge over the sample area. For the coating design #2, the wavelength position of a local minimum of the reflectance was evaluated, e.g. at 588 nm. The uniformity was confirmed by measurements on single layers. With those values and the theoretical design, the reflected phase spectra are calculated. The peak-to-valley wavefront error results from the maximal difference in the reflected phase, taken wavelength by wavelength. In order to obtain RMS WFEs, the data is divided by a factor of 6.

In contrast to the method presented in [12], here also the additional effect of the non-uniform air layer is included. The result shows in Figure 8, right (black line). The red triangles in Figure 8 (left) do not include this effect. The effect of the non-uniform air layer results from the non-uniform coating, separately from the interference effect. In the case of the coating #2, for the non-uniformity of $\pm 0.125\%$, and the thickness of 14.2 μm , the thickness of the air layer is 35.5nm, resulting in an additional peak-valley wavefront error of 71nm (12nm rms).

In Figure 8, right, spectrally resolved wavefront measurements of the beamsplitter #2 were performed in the wavelength range of 400-800 nm in 2-5 nm intervals. Due to chromatic aberration of the expansion optics and the associated spot shift on the Hartmann-Shack sensor the relative wavefront errors were sectionally evaluated, referencing the data to the largest wavelength of each section. The chromatic aberration was corrected by means of a regression line, which was subtracted from the measured data in each section. Note that the relative method is unable to measure the WFE absolutely, so it needs a reference. The referencing of the relative WFE measurement was done spectrally linear, so that they fit with the absolute WFE data (green triangles). As seen from Fig. 8 (red dots) no significant features in the corrected relative WFE can be

observed within the measuring accuracy of ± 5 nm RMS. At two selected wavelengths absolute WFE referenced to the Zygo flat were recorded (green triangles in Figure 8, also in Figure 9). The absolute WFE data were corrected with the effects of the substrate holder by measurements at different azimuthal angles of the sample. Also the WFE data are corrected by the gravity-bending by a separate measurement of an identical uncoated substrate. Thus, although the WFE is corrected by gravity and chromatic effect, it still includes the residual bending of the substrate due to different film stress of the two coated sides. Both the low values of the absolute WFE and the agreement with theory indicates how precise the stress compensation of the component works, i.e. within the measurement accuracy, no space is left for residual stress bending of the component.

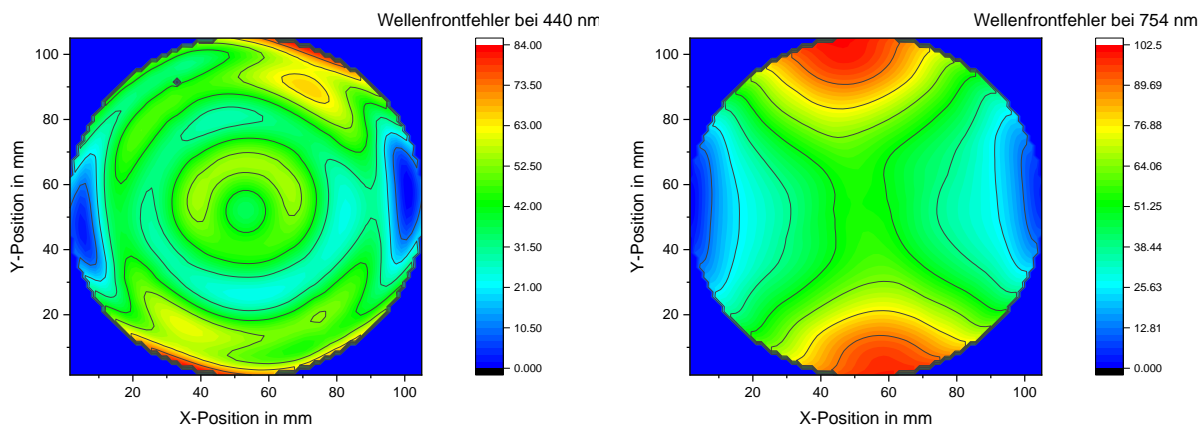


Figure 9: Absolute wavefront error maps of the beam splitter #2 measured with Hartmann-Shack sensor at 440 nm (left) and 755 nm (right), respectively. The WFE maps are corrected from sample holder features and also from chromatic effects.

4.2 Bandpass coating

The bandpass filter was fabricated in the EOSS[®] coater, too. It is applied onto the convex surface of a spherical lens with a lateral diameter of 25 mm and a curvature radius of 25.84 mm. A position of 4.8 mm apart from the center is specified as off-center position. The lens is tilted by 5° . The surface has an angle of another 11° . In summary, an angle of 16° results for which the coating has to be compensated. To correct for this angle, the coating needs to be thicker by about 1.6% at the off-center position.

In physical vapor deposition processes, the deposition rate depends on the distance between source and substrate and is also proportional to the cosine of the angle between surface normal and deposition flux [11]. For the given lens geometry, this leads to a natural decrease of the film thickness by about 8% from the lens center to the outmost position. In contrast, the goal for optimal correction of the interference filter behavior is a linear *increase* of 3.4% between center and outmost position, which would yield the required 1.6% at the specified position.

This goal is realized by using a spinning lens substrate together with a shaping mask in form of a sharp spike, coinciding with the position of the lens center. This way, an increase of the sub-rotation averaged thickness profile from center to border of the lens can be achieved. In order to rotate the lenses during the coating process, a corresponding holder was designed and manufactured. This lens holder is attached directly to a direct current motor. Depending on the applied voltage, the rotational speed can be changed. The rotational speed of the sub-rotation is approximately 2000 revolutions per minute. To protect the components from excessive temperatures various heat shields are provided.

Finding an optimized geometric setup with respect to shaper geometry and alignment (e.g. distance between shaper and lens etc.) is not trivial. For this reason, we carried out a simulation study prior to experimental realization. The simulation model is based on the reactor model of the EOSS[®] coater presented in [10]. In this model, a uniform sputter erosion profile is assumed throughout the racetracks of the cylindrical targets, and the gas flow and transport of sputtered atoms is obtained by Direct Simulation Monte Carlo (DSMC) method. For the deposition profile on flat substrates, it was

sufficient to take the vertical component of the DSMC computed sputter flux and integrate it along the circular tracks of the turntable motion.

For convex substrates, this approach does not work anymore. Instead, we sample the DSMC computed deposition flux in a plane located a few mm below the substrate trajectory with lateral and angular resolution. The projection of the angularly resolved flux profile onto the moving 3D substrate is accomplished via a ray-tracing approach similar as in [11] across the remaining distance to the substrate. Furthermore, the actual problem requires shaping masks with sharp geometric features. Under such conditions, it turned out that the assumption of a uniform sputter profile does no more yield satisfactory agreement with the experiment. Therefore, we performed a Particle-in-Cell Monte-Carlo (PIC-MC) plasma simulation for determination of a more realistic sputter profile as input for a subsequent DSMC simulation of the sputtering process. A detailed description of the respective simulation modules will be published elsewhere.

Based on the modelled deposition rate, shaper mask geometries are optimized via fitting geometric coordinates and curvature radii with respect to the linear film increase goal. At the same time, another part of the shaper mask is adjusted for yielding a uniform profile on a flat monitor substrate. The combined mask design together with modelled resulting deposition profiles shows the left graph of Figure 10, while the right graph shows to measured spectra of a bandpass filter on a lens taken from the center and the off-centered position as specified above. It is demonstrated that a low spectral shift occurs between both positions. It has to be noted that still there is a difference between expected and realized deposition rate. For the Ta_2O_5 the rate is 3,5% higher and for SiO_2 it was about 2% lower. Tooling factors were introduced to compensate this effect. A number of runs confirmed the rate difference, i.e. effects due to inaccurate mounting of components can be ruled out. One reason of the difference in deposition rate might be the different behavior of the two materials with respect to the angular behavior, which is at the moment not included in the model.

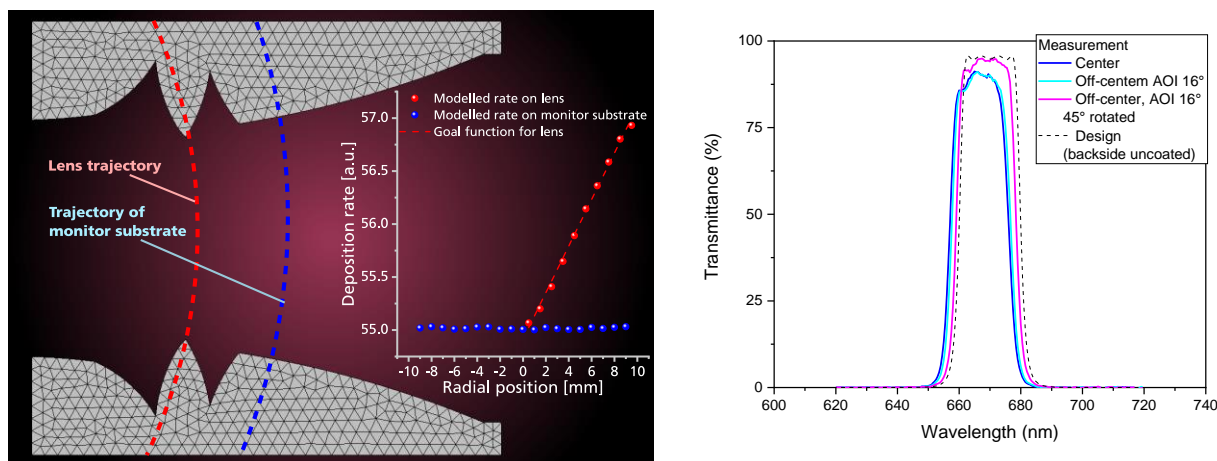


Figure 10: Model-based design of shaper masks and modelled resulting deposition profiles on lens surface and monitor substrate (left) and spectra of a bandpass filter coated on a lens substrate taken from center and two different off-center positions $r=4.8$ mm (right).

5. SUMMARY AND CONCLUSION

In the present paper, a broadband beam splitter coating with a reduced wavefront error was developed. Spectral wavefront errors occurring in broadband beam splitter coatings were studied both theoretically and experimentally. With the use of a commercial design program, dielectric coatings with reduced spectral WFE were designed, using the group delay as a target parameter. A coating design is found that exhibits a significantly smaller WFE compared to a coating where only the spectral properties were used as a design target. However, it is found that for a given non-uniformity, a low wavefront error requires thinner coatings, while the spectral requirements require more complex and thicker designs. Different coatings with low losses were deposited accordingly using the EOSS[®] magnetron sputtering system. For qualification of the beam splitter a new measurement setup based on a Hartmann-Shack wavefront sensor was developed. It allows for spectrally resolved wavefront measurements from 400nm to 800nm with a spectral bandwidth of 2nm. The method is very

fast because only the variation of the wavelength is needed for a without moving or replacing the components or the substrates. However, the relative method needs referencing. This was done with the Hartmann-Shack sensor, too. Therefore, errors caused by gravitational bending of the sample and by chromatic effects of the setup were compensated. A good agreement between measurement and theory was found. The spectral WFE was measured to be about 20nm within the accuracy of the measurement.

A combination of a sub-rotation with a shaping mask was used to deposit the lens by magnetron sputtering with the EOSS® turntable coater. For theoretical analysis of the coating profile, the 3D plasma of the magnetron discharge in the sputter compartment was simulated with a particle in cell Monte Carlo Simulation code [Pflug2013]. A good agreement between predicted uniformity and experiment can be obtained, provided that the plasma is carefully simulated in 3 dimensions. Residual deviations are likely due to inaccurate angular dependence of the sputter profiles of the Silicon and the Tantalum materials, respectively. The difference between theory and experiment is typically about 2%. A bandpass filter with spectral shift less than a few nm could be fabricated.

ACKNOWLEDGEMENT

The results presented in this study were obtained in a study funded by ESA under contract no. ITT AO/1-541/15/NL/PS.

REFERENCES

- [1] Knowlden, R. E., "Wavefront errors produced by multilayer thin-film optical coatings", AA (Arizona Univ., Tucson), Ph.D. Thesis Arizona Univ., Tucson. 1981.
- [2] Nyland, K., Jurgenson, C.A., Buscher, D.F., Haniff, C.A., Young, J.S., Lewis, J., Schnell, R., "Custom Beamsplitter and AR Coatings for Interferometry", Society of Photo-Optical Instrumentation Engineers (2010).
- [3] Venancio, L. M. G., Carminati, L., Alvarez, J. L., Amiaux, J., Bonino, L., Salvignol, J.-C., Vavrek, R., Laureijs, R., Short, A., Boenke, T., Strada, P., "Coating induced phase shift and impact on Euclid imaging performance", SPIE Astronomical Telescopes + Instrumentation (2016) 99040V.
- [4] M. Lappschies, T. Weber, L. M. Venancio, and S. Jakobs, "Advanced dielectric coatings for the Euclid mission telescope manufactured by the PARMS process," in Optical Interference Coatings 2016, OSA Technical Digest (online) (Optical Society of America, 2016), paper MC.2.
- [5] Baumeister, P., Optical Coating Technology, SPIE Press, Bellingham, WA (2004).
- [6] Wyant, J. C., Creath, K., "Basic Wavefront Aberration Theory for Optical Metrology", Chapter 1, APPLIED OPTICS AND OPTICAL ENGINEERING, VOL. XI, Academic Press Inc., (1992), ISBN 0-12-408611-X
- [7] McLeod, A., "Phase Matters", 31 May 2005, SPIE Newsroom. DOI: 10.1117/2.5200506.0008,
- [8] Rademacher, D., Bräuer, G., Vergöhl, M., Fritz, B., Zickenrott, T., "New sputtering concept for optical precision coatings", Proc. SPIE 8168, Advances in Optical Thin Films IV, 81680O (4 October 2011); doi: 10.1117/12.896843; <https://doi.org/10.1117/12.896843>
- [9] Vergöhl, M., Bruns, S., Rademacher, S., Bräuer, G., "Industrial-scale deposition of highly uniform and precise optical interference filters by the use of an improved cylindrical magnetron sputtering system", Surface and Coatings Technology, Volume 267 (2015), Pages 53-58, ISSN 0257-8972,, <https://doi.org/10.1016/j.surfcoat.2015.01.051>.
- [10] Pflug, Andreas; Siemers, Michael; Melzig, Thomas; Rademacher, Daniel; Zickenrott, Tobias; Vergöhl, Michael, Numerical optimization of baffles for sputtering optical precision filters, Surface and Coatings Technology (2013), 10.1016/j.surfcoat.2013.11.008
- [11] Deppisch, G., Schichtdickengleichmäßigkeit von aufgestäubten Schichten - Vergleich zwischen Berechnungen und praktischen Ergebnissen. Vakuum-Technik, Volume 30 (1981), Pages 106-114.
- [12] Michael Vergöhl, Chris Britze, Stefan Bruns, Jennifer Ahrens, Bernd Schäfer, Klaus Mann, Volker Kirschner, "Development of a broadband dielectric beam splitter with reduced spectral wavefront error," Proc. SPIE 10691, Advances in Optical Thin Films VI, 1069118 (6 June 2018)